NATIONAL AERONAUTICS AND SPACE ADMINISTRATION

Research Grant NGR-09-005-025

Diagnostics of Accelerating Plasma

6th Semi-Annual Progress Report

September 1, 1968 - February 29, 1969

Report No. 69-001

by

T.N. Lie and E.A. McLean

May 31, 1969

Department of Space Science and Applied Physics

The Catholic University of America

Washington, D.C. 20017

Foreword

The present semi-annual progress report consists of two separate studies, i.e., 1) Validity criteria of the Local Thermal Equilibrium Assumption in Electromagnetic Shock Tubes, 2) Current-sheet Velocity in a Coaxial Plasma Accelerator. The former study will be presented at 7th International Shock Tube Symposium, Toronto, Canada, on June 23-25, 1969 and the latter was presented at AIAA 7th Electric Propulsion Conference, Williamsburg, Va., March 3-5, 1969. The latter study is a revised and extended version of the 4th semi-annual progress report. Authors wish to acknowledge the contribution made to this report by M.J. Rhee, a graduate assistant.

ABSTRACT

A validity criteria for LTE are applied to the T-tube plasma in order to justify the result described in the previous semi-annual report. Furthermore, the line intensities of He II 4686 Å and He I 5876 Å are calculated under the assumption of LTE in order to compare the values with those obtained from the measurement. The two results indicate that the T-tube plasmas with $N_e > 10^{17} cm^{-3}$ are in approximate LTE and those with $N_e < 10^{17} cm^{-3}$ may deviate from LTE density population.

Several factors which affect the velocity of the current-sheet in a coaxial plasma accelerator such as the insulator ablation, the radius ratio of the electrode, the species of gas and its pressure are examined experimentally and the results are compared with the theoretical predictions.

TABLE OF CONTENTS

LIST OF ILLUSTRATION

I. Validity of the Local Thermal Equilibrium Assumption in Electromagnetic Shock Tubes

A. Introduction

In the previous semi-annual report, the electron temperature determined using two techniques has been compared, namely, one technique which is strongly dependent on the Local Thermal Equilibrium (LTE) assumption and one which is independent of the LTE assumption. These measurements were made on a reflected and incident shock wave produced in an electromagnetic T-tube which has been pre-filled with helium or hydrogen to a pressure of 0.5 to 1 torr. Within the experimental uncertainty of $\pm$ 15 percent, the two temperatures were shown to agree, indicating that the assumption of LTE used in the spectroscopic temperature determination is a reasonable approximation.

In this report, a validity criteria for LTE given previously are applied to the present experiment in order to justify the experimental result obtained. Furthermore, the line intensities of He II 4686 Å and He I 5876 Å are calculated under the assumption of LTE in order to compare the values with those obtained from the measurement. These are made at various distances from the electrodes of the T-tube including a location very close to the arc. The result indicates that the two values of line intensity agree very well at 2 cm (z = 2 cm) from the arc where the electron density is rather high ($N_e = 3.5 \times 10^{17} cm^{-3}$). On the other hand, there is discrepancy of a factor of 2-3 between the calculated and measured values at z = 6 cm and z = 12 cm meaning that the population density may deviate from the LTE population. However, this deviation would cause an error in the temperature determination of only $\sim$ 15 percent.

B. Validity Criteria for LTE

The concept of local thermal equilibrium, in which temperature is the most important parameter, is a special case of complete thermodynamic equilibrium as examplified by a black body radiator and Planck's radiation law. For an optically thin plasma with sufficient numbers of particles so that collisional processes are much more frequent than radiative processes, one can neglect the losses due to radiation and still be able to apply the Boltzmann and Saha relations to calculate population densities of the various component particles and the populations of the excited states, and the Einstein coefficients to relate radiation intensities to temperature and densities.

Griem[1] and others[2,3] have derived useful validity formulas which can be applied to plasmas to determine when the local thermal equilibrium assumption can be used, provided approximate electron densities and temperatures of the plasmas are known. First, we consider the validity criterion for LTE in a homogeneous transient plasma. It is necessary to ascertain if the relaxation for the establishment of LTE is smaller than the time variations of the densities and the temperature. The plasma that is being observed is relatively homogeneous perpendicular to the axis of the tube, i.e., along the line of sight (except the thin boundary layer) and has only gradual variations along the tube axis. Since collisional ionization occurs mainly via intermediate excited states (stepwise ionization), the ionization relaxation time is determined by the slowest process in the excitation chain, i.e., the excitation from the ground state to the upper state of the resonance line. This relaxation time, including a factor for the equilibrium fraction of atoms or ions in the next stage of ionization, is given by Griem[1] as

$$\tau_1^{z-1} \approx \frac{1.1 \times 10^7 z^3 N^z}{f_{21} N_e (N^z + N^{z-1})} \frac{E_2^{z-1}}{z^2 E_H} \left(\frac{kT}{z^2 E_H}\right)^{1/2} \exp\left(\frac{E_2^{z-1}}{kT}\right) \text{sec} \qquad (1)$$

Here, z is the number of effective charges acting on the radiating electron, (z = 1 for an atom, z = 2 for a singly charged ion, etc.), E_H is the ionization energy of hydrogen, f_{21} is the absorption oscillator strength of the resonance line, N_e is the electron density, E_2^{z-1} is the excitation energy of the resonance line, and N^z, N^{z-1} are the particle densities of the indicated degree of ionization.

A calculation of the relaxation time to establish first ionization yields times (10^{-8} - 10^{-7} sec) usually much shorter than the plasma lifetime (approximately 1 μsec). Also, collisional-radiative calculations[4], show that the bound states of He I are in local thermal equilibrium; however, the question is whether population of excited states of He II and the number of He III ions is in LTE relative to the ground-state population of He II. A calculation of the relaxation time for second ionization yields values ranging from 0.3 μsec for $N_e \geq 10^{17}$ to several microseconds for the lower values of N_e. However, the plasma lifetime may be lengthened because the excited particles are carried along the plasma. Generally, then it must be said that the Griem LTE criterion is only marginally met in the higher density cases, and is not fulfilled in the lower density cases.

In addition to the first validity criterion for LTE described above, it is necessary to fulfill the criterion for LTE in a homogeneous and time-independent plasma. If the resonance line is optically thick, as is usually the case for such plasmas, this criterion for the electron density is

$$N_e \geq 9 \times 10^{16} \left(\frac{E_2^{z-1}}{E_H}\right)^3 \left(\frac{kT}{E_H}\right)^{1/2} \text{cm}^{-3} \qquad (2)$$

with the same meaning for the symbols as in the previous equation. If this criterion is fulfilled, the population of the ground state is in LTE with respect to higher levels to about 10 percent. A typical example of the electron densities necessary for complete LTE to within a factor of 2 or 3 (rather than the 10 percent) for ionized helium with optically thick resonance lines at kT = 4 eV would be $N_e \approx 10^{17}$ cm^{-3}. Our experimental electron densities are approximately within this range. A similar result has also been obtained by Mewe[5].

C. Spectroscopic Measurement

Isler and Kerr[6] and Cloupeau[7] maintain that the radiation from the luminosity front comes from gas excited primarily in the discharge rather than gas which has been heated by the shock wave. Because of this, Isler and Kerr feel that the temperature is decreasing too rapidly to permit the ion concentration in the plasma to relax to their steady state values. In order to ascertain if the plasma behind the shock in the T-tube is a recombining plasma in which the heating has been done solely in the arc region, spectroscopic measurements were made of T_e and N_e at various distances from the discharge (see Fig. 1). The temperature was measured from the line intensity ratio of He II 4686 Å and He I 5876 Å and the electron density was determined from the Stark line profiles of these two lines using the theoretical calculations of Griem, et.al.[8]. Fig. 2 shows typical line profile of He II 4686 Å measured at a location of z = 2 cm. The values thus obtained are $T_e = 4.1$ eV, $N_e = 3.5 \times 10^{17}$ cm^{-3} at z = 2 cm, $T_e = 3.7$ eV, $N_e = 6.8 \times 10^{16}$ cm^{-3} at z = 6 cm and $T_e = 3.7$ eV, $N_e = 5.4 \times 10^{16}$ cm^{-3} at z = 12 cm. The propagation velocity of the luminous front is measured using a streak photograph of

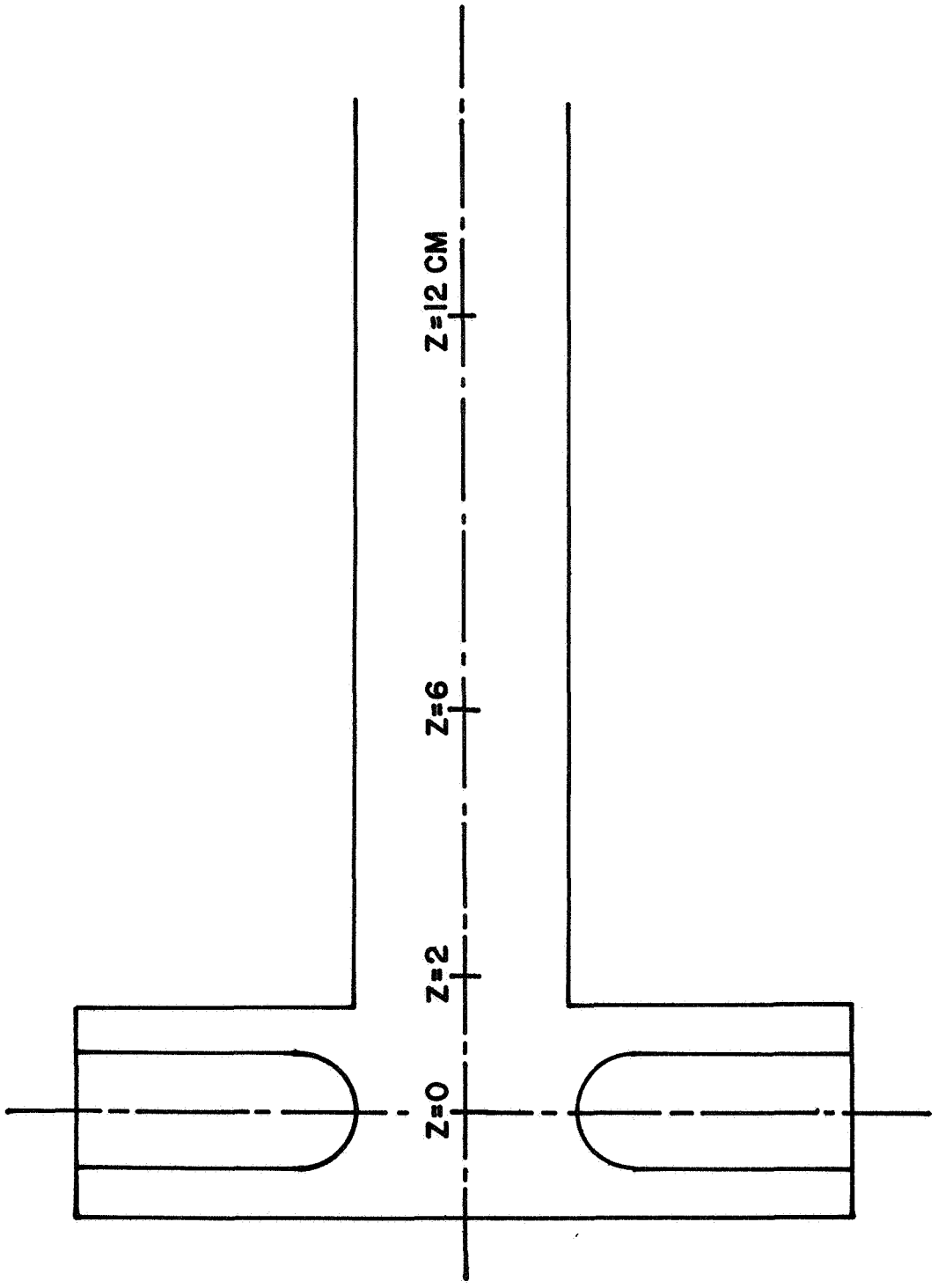

FIG. I LOCATIONS OF SPECTROSCOPIC MEASUREMENT

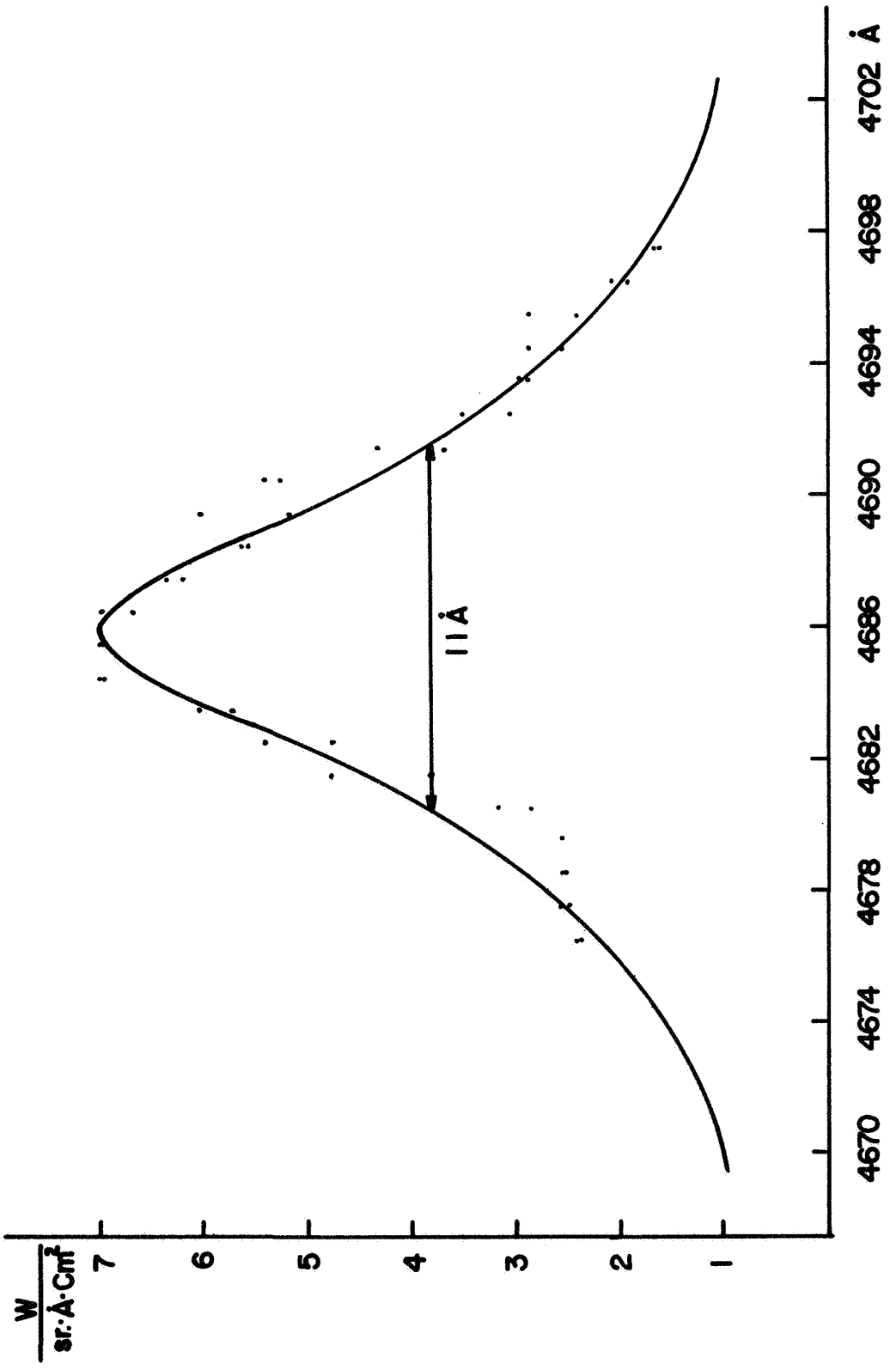

FIG. 2 STARK LINE PROFILE OF He II 4686 Å AT Z = 2 CM.

an image converter camera and the velocity as a function of z is shown in Fig. 3. One sees the velocity peak at z = 6 cm and it is found that this is the location where the loop of the arc current ruptures toward the downstream of the side arm. The above measurements show that the electron temperature (measured spectroscopically) near the arc is only slightly higher than that at z = 12 cm or within the time interval of about 2.5 μsec. Furthermore, it is found that the laser scattering temperature at z = 12 cm is higher by ~ 0.4 eV than the spectroscopic temperature at the same location. Since the laser scattering temperature near the arc may be the same as the spectroscopic temperature due to the existence of LTE, the temperature difference between the arc region and the 12 cm location may be even smaller. The data presented here corresponds to a lower temperature in the arc region than originally expected[9] and the decay in temperature is not as fast as one would expect even for a simple adiabatic expansion. Thus it appears that the plasma here is not only heated by the arc, but is also continually heated by the shock wave that forms at the leading edge of the plasma, although for these conditions the shock wave does not separate from the driver gas[10].

Absolute line intensities of He I 5876 Å and He II 4686 Å have been measured at z = 2 cm, 6 cm, and at 12 cm, respectively in order to compare the calculated values. The total line intensity was obtained from the line profiles measured on a shot-to-shot basis with a monochromator. The monochromator was calibrated using a standard tungsten ribbon-filament lamp. In order to calculate the line intensity, the optical path length through which spectroscopic measurements are made must be known. At z = 6 and 12 cm the path length is approximately the inner diameter of the T-tube; however, it is much smaller than the tube diameter at z = 2 cm as is shown in Fig. 4.

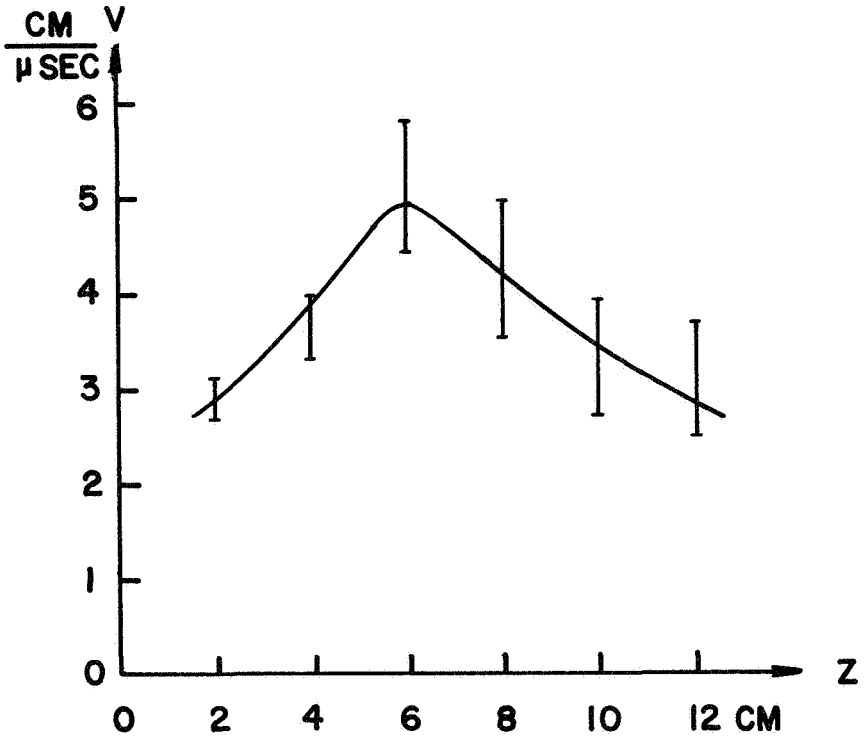

FIG. 3 VELOCITY V S. DISTANCE Z

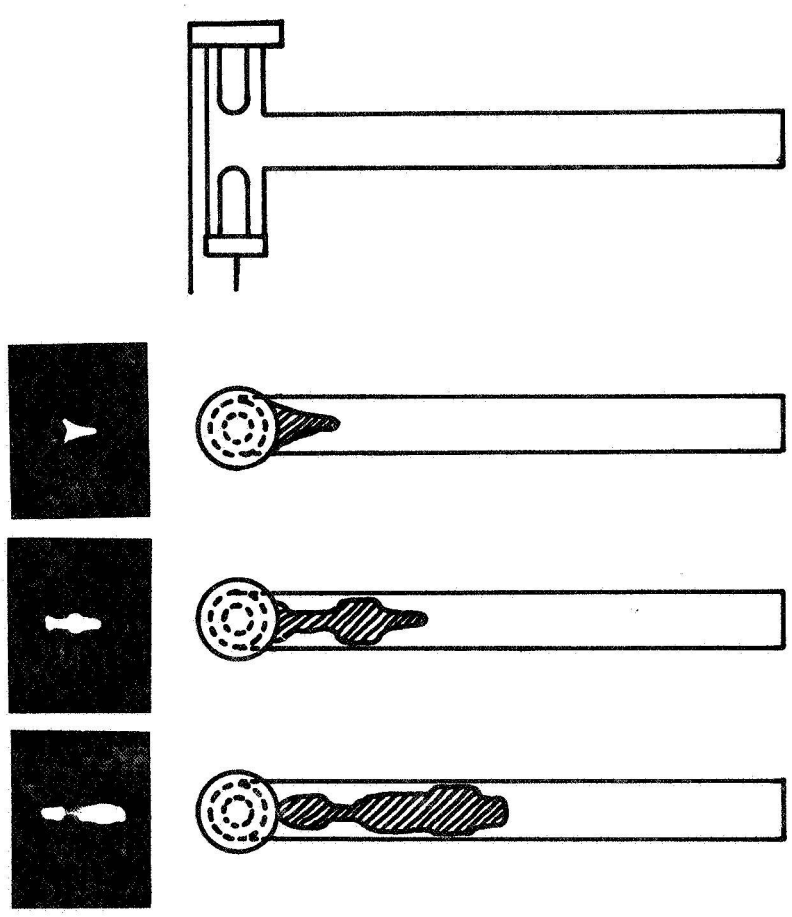

FIG. 4 FRAMING PHOTOGRAPHS SHOWING OPTICAL PATH LENGTH OF PLASMA.

D. Calculation of Total Line Intensity

A degree of deviation from LTE may be estimated by comparing the measured total line intensity with that calculated under the assumption of LTE. For plasmas in thermodynamic equilibrium, the ratio of the total density between atoms or ions of the same chemical species in two subsequent ionization stages is given by Saha equation,

$$R^z(T) = \frac{N^{z-1} N_e}{N^z} = \frac{2Z^{z+1}(T)}{Z^z(T)} \left(\frac{mkT_e}{2\pi\hbar^2}\right)^{3/2} \exp\left(-\frac{E_\infty^z - \Delta E_\infty^z}{kT_e}\right), \tag{3}$$

where N^z = number density of z-fold atoms

$Z^z(T)$ = partition function of z-fold ionized atom

m = electronic mass

E_∞ = ionization energy

ΔE_∞ = reduction in ionization energy

ΔE_∞ is a small correction of the ionization energy due to electric microfields in the plasma and is given by

$$\Delta E_\infty = 6.24 \times 10^{11} (z + 1) \frac{e^2}{\rho_D} \quad \text{eV} \tag{4}$$

where

$$\rho_D = \left[\frac{kT_e}{4\pi(N_e + \sum_{a,z} z^2 N_a^z)\, e^2}\right]^{1/2} \quad \text{cm} . \tag{5}$$

Defining a reduced Saha equation $R^{z*}(T)$

$$R^{z}(T) = \frac{2Z^{z-1}(T)}{Z^{z}(T)} \; R^{z*}(T)$$

$$R^{z*}(T) = \left(\frac{mkT_e}{2\pi\hbar^2}\right)^{3/2} \exp\left(-\frac{E^{z}_{\infty} - \Delta E^{z}_{\infty}}{kT_e}\right) \tag{6}$$

$R^{*z}(T)$ has been calculated and tabulated for different values of T and different values of ΔE_{∞} by Drawin and Felenbok[11]. From $R^{z*}(T)$, one obtains the number density ratio of successive ionization stage, i.e.,

$$\frac{N^{z+1}}{N^{z}} = \frac{2Z^{z+1}}{Z^{z}} \; \frac{R^{z*}(T)}{N_e} \tag{7}$$

For the helium plasma, the number density of singly ionized helium atoms is obtained assuming quasi-neutrality condition, i.e.,

$$N_e = N^{+} + 2N^{++} \tag{8}$$

Table I gives the optical layer length l, the measured values of T_e and N_e, and the value of N^{+} at three different distances from the arc. With this information, the line intensities of He II 4686 Å and He I 5876 Å are readily obtained from the following equation,

$$I^{0,+}_{mn} = \frac{2\pi e^2 h(\nu^{o,+}_{mn})^3}{mc^3} \; \frac{g_n{}^{o,t}}{Z^{o,+}} \cdot f^{o,+}_{mn} \cdot l \cdot N^{o,+} \exp\left(-\frac{E^{o,+}_{m}}{kT}\right) , \tag{9}$$

where 0 refers to the neutral line and + refers to the ion line. The calculated values of the total line intensities are tabulated in the Table I together with those measured for comparison. It is seen that the intensity at 2 cm from the arc gives a good agreement of measured and calculated values, whereas, at z = 6 cm and z = 12 cm the calculated values

Table I Comparison of total line intensity of He II 4686 measured and calculated under the assumption of LTE

z		T_e	N_e	N^+	He I 5876	He II 4686	He II 4686
cm	cm	eV	cm^{-3}	cm^{-3}	measured	measured	calculated
					watts $sr^{-1}cm^{-2}$		
2	0.9	4.1	3.5×10^{17}	2.7×10^{17}	40	82	79
6	2.8	3.7	6.8×10^{16}	5.3×10^{16}	15	29	13
12	2.8	3.7	5.4×10^{16}	4×10^{16}	13	30	9

differ from the measured values by a factor of 2-3. This indicates that the plasma near the arc where the electron density is as high as 3.5×10^{17} cm^{-3} may be in LTE but there could be a deviation from a LTE population density distribution further down the tube of a factor of 3 due to a much lower electron density ($5 \times 10^{16} cm^{-3}$). However this deviation would lead to an error in the temperature measurement of only $\sim$ 15 percent as was described in the previous annual progress report.

E. Conclusion

The calculated relaxation times for excitation and ionization of the singly charged helium ion behind the shock, are shorter than the plasma lifetime in the case of $N_e > 10^{17} cm^{-3}$ and vice versa in the case of $N_e < 10^{17} cm^{-3}$. The validity criterion for LTE in the time-independent plasma again shows the electron density to be $N_e > 10^{17} cm^{-3}$. The comparison between the calculated and the measured line intensities of He I and He II lines indicates good agreement near the arc region where the electron density is $3.5 \times 10^{17} cm^{-3}$ and a factor of 2-3 disagreement further down the side arm. Using the same method for comparison as Isler and Kerr[6], the ratio of doubly charged to singly charged ion density is found to be the same as the LTE ratio within a factor of two-well below the several orders of magnitude which they claim.

II. Current-sheet Velocity in a Coaxial Plasma Accelerator

A. Introduction

The propagation velocity of the current-sheet in a coaxial plasma accelerator is, in general, limited, i.e., the velocity does not increase beyond a certain value even if the total energy input to the accelerator is greatly increased. The velocity limitations of the current-sheet in a coaxial accelerator have been investigated by a number of authors previously. Thom et al[12] suggested that a drag force associated with ions striking the cathode acts on the accelerating plasma. The velocity drag depends on the ion-electron partition of the current-sheet and also on the atomic weight of the ambient gas used. Keck[13] proposed that the velocity limitation observed in his magnetic annular shock tube may be due to insulator ablation. The ionized vapor of ablated material near the insulator wall provides the current path and the additional mass introduced by the vapor contributes as an inertial drag.

The former[12] drag is only significant in a case where a heavier gas such as argon or air is used as the working gas and is negligibly small with lighter gases. Therefore it does not account for the velocity limitation observed with lighter gases[13]. The velocity drag due to the insulator ablation on the other hand, could be a serious one regardless of the working gas used if Keck's physical model on the ablation is relevant.

The ablation drag was treated analytically by Workman[14] using a steady flow model very similar to that of Keck. His results shows that the ablation loss can be expressed with a single correlation parameter which specifies the magnetic piston velocity

as a function of the total magnetic field, the initial gas density, and the ionization potential of the insulator material. However, the theory requires a thorough experimental check in order to be generally accepted.

In this report, first, the current-sheet velocities in two groups of coaxial plasma accelerators with refractory and non-refractory insulators are compared in a wide variety of operating conditions, in order to confirm the existence of a velocity drag due to ablation. This has not been done previously to the best of our knowledge. Secondly, the primary ablation process predicted by Keck is examined using a magnetic probe, monochromators and an image converter camera. Thirdly, Workman's theory on the ablation loss is compared with the measurements obtained in this study.

An analytical expression for the current-sheet velocity has also been examined experimentally by varying several parameters of the coaxial accelerator.

B. Velocity Drag Due to Insulator Ablation

The dimensions of the coaxial plasma accelerators used in this investigation are listed in Table 2 with their schematic diagram. The three accelerators used differ only in the inner electrode diameters - the outer electrode diameter is kept the same. The length of the electrodes is 22 cm. Two slots, 1 mm wide and 15 cm long, are provided on the outer electrode along the accelerator axis for the optical measurement. The insulator which separates the two cylindrical electrodes at the accelerator breech has the shape of a flat circular disc with a hole at the center. The insulating materials used so far are lucite, mylar, alumina, pyrex and vycor glass and these are easily interchanged by removing the inner electrode. The accelerator electrodes are enclosed by a vacuum chamber 9 inches in diameter and 60 inches long which is made of plexiglass.

TABLE 2 Dimensions of Coaxial Plasma Accelerator

Accelerator	Dia. of O.E. (mm)	Dia. of I.E. (mm)	Insulator
7A	60	22	Mylar, Lucite Pyrex and Vycor Glass
7B	60	32	Pyrex Glass, Lucite
7C	60	40	Lucite

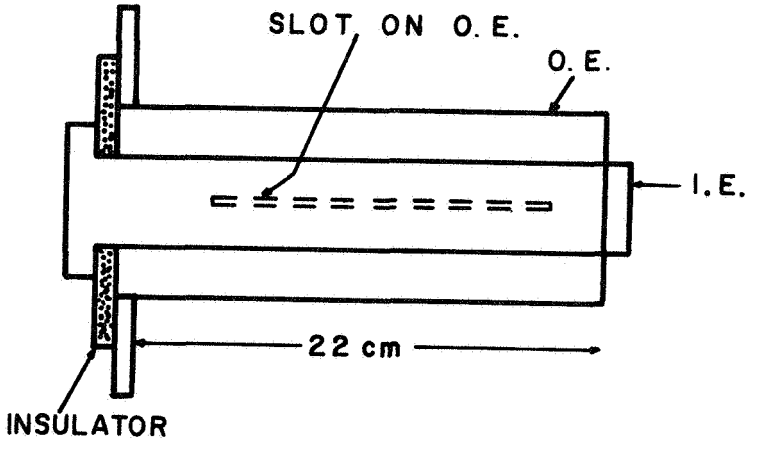

A 60 μF capacitor is charged to 10 kV and the discharge is initiated by triggering a vacuum spark switch[15]. The quarter cycle time of the discharge is about 3.5 μsec. The maximum discharge current with a 10 kV charging voltage is about 160 kA. The accelerator is operated with a static filling rather than with an injection of propellant gas. The working gases used are hydrogen, helium, nitrogen, and argon in the pressure range of 0.03 to 1.5 torr. The base pressure of the vacuum chamber prior to the gas filling is always below 1 mtorr, and after each shot the chamber is evacuated and refilled to insure the purity of the gas.

Most of the experimental measurements in the present investigation consist of accurate determinations of the luminous front velocity from streak photographs taken of the moving plasma through the slot in the outer electrode. An image converter streak camera is used for the photography. Since the velocity of the luminous front varies with time as the discharge current increases, the velocity measurements are made at a fixed phase or a fixed time of the discharge cycle rather than at a fixed position of the accelerator barrel. This is monitored by oscillograms of the discharge current and the image converter streak monitoring signal from the camera simultaneously. Figure 5 shows a typical streak photograph and oscillograms of the discharge current and the streak signal recorded simultaneously. As can be seen, the luminous front is usually well defined for the gas pressure range used in this investigation. The shot-to-shot reproducibility of the measurement is 10 percent or better in most cases. One notices bright second fronts in the photograph which have approximately the same velocity as first front. As already reported in a previous report[16], the first and second front in the streak photograph correspond to the portions of the current-sheet which intersect with the

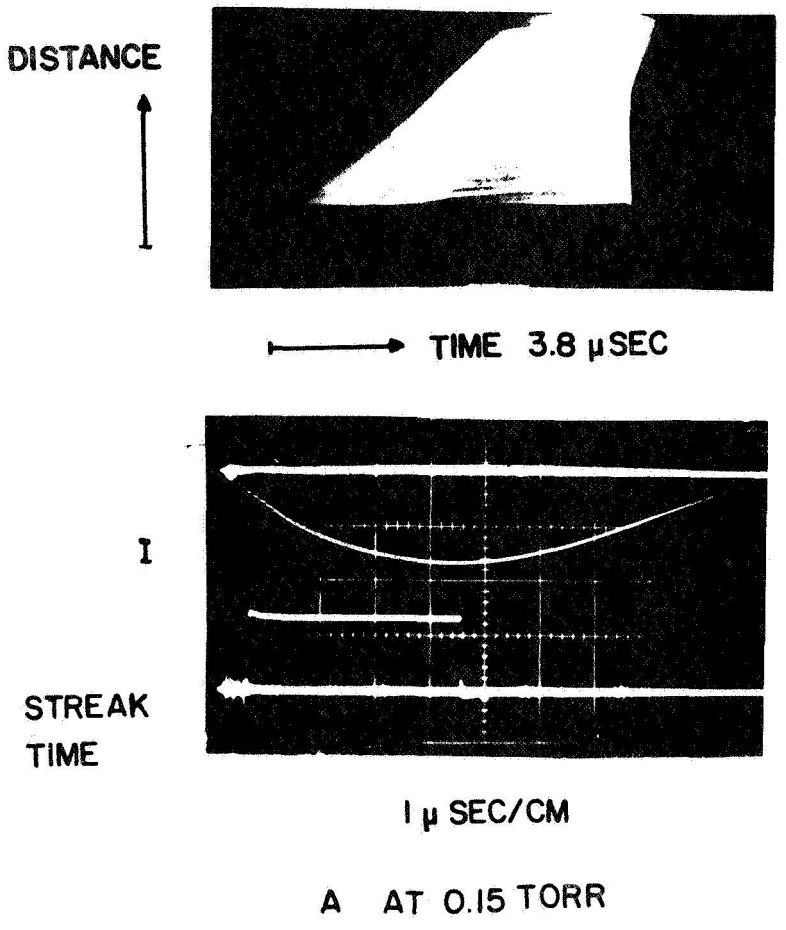

FIG. 5 STREAK PHOTOGRAPH OF LUMINOUS FRONT AND SIMULTANEOUS RECORDING OF TOTAL DISCHARGE CURRENT AND STREAK MONITOR SIGNAL.

with the inner and the outer electrode respectively. The second front is usually brighter than the first front because this part of the current-sheet, along the outer electrode wall, forms a well-defined ring where the electron density is rather high.

In order to avoid further complications, the accelerator geometry is kept the same while the insulators are changed from one material to another for comparison. Four different insulator materials are used with Accelerator 7A and the sheet velocities are measured at fixed capacitor charging voltage. The result is shown in Fig. 6, where the measured velocities are plotted against the filling pressure of nitrogen and hydrogen. The velocities corresponding to the trials with insulator materials of lucite and mylar given approximately the same value in the pressure range used here. The velocities with vycor and pyrex glass are also very close to each other within the experimental scatter. However, one notices a large velocity difference between the two groups of insulators, i.e., velocities with a lucite insulator give about 65-70 percent of that with vycor glass. It should also be noted that all curves (regardless of the insulator material) follow approximately the snowplow prediction $U \propto p^{-4}$, where U and p are the measured velocity and the initial gas density, respectively.

C. Process of Insulator Wall Ablation

The velocity difference observed in the accelerator with refractory and non-refractory insulators is almost certainly caused by the ablation from the insulator wall. Keck[13] has predicted that the inertial drag of material ablated from the walls is the main source of the velocity limitation in an accelerator where non-refractory material is used. According to him, the ablation of the insulator wall takes place in the early

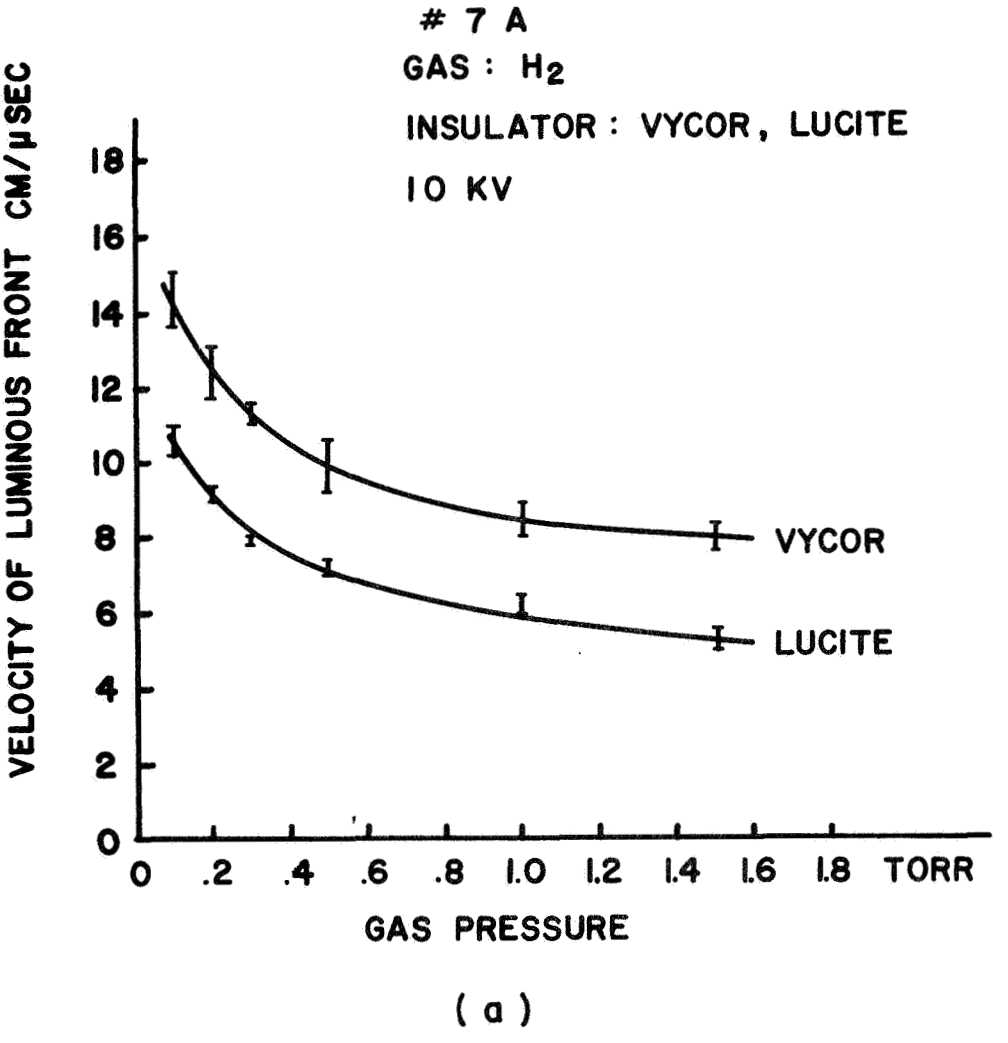

FIG. 6 COMPARISON OF VELOCITIES IN ACCELERATOR 7A WITH REFRACTORY AND NON-REFRACTORY INSULATOR. (a) WITH HYDROGEN GAS

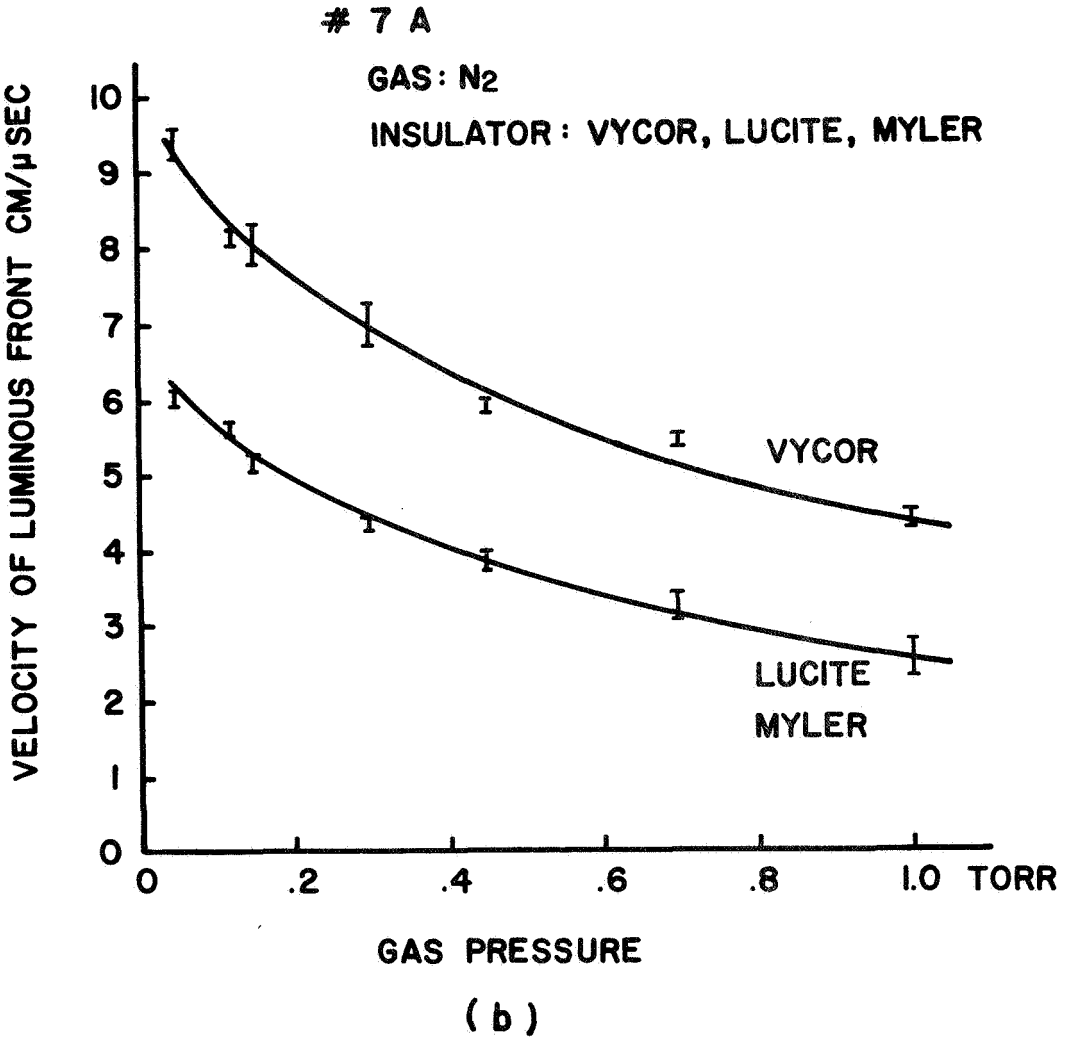

FIG. 6 COMPARISON OF VELOCITIES IN ACCELERATOR 7A WITH REFRACTORY AND NON-REFRACTORY INSULATOR. (b) WITH NITROGEN GAS.

stage of the discharge. The material from the wall is rapidly ionized and, since it is at rest in a strong electric field, a current will flow, causing both joule heating and an acceleration of the ablated material. A well-confined standing arc is formed close to the insulator wall and in turn transfers a portion of its heat (or energy) back to the insulator end-wall, thus generating a continuous flow of vapor from the wall. Only a portion of the total discharge current would flow in the current-sheet under this circumstance, resulting in a reduction in the sheet velocity.

A qualitative check on Keck's ablation model is made experimentally. First, in order to examine the existence of ablated material flow behind the current-sheet, two monochromators are focused through the slots in the outer electrode at two separate axial locations of the accelerator barrel. The line of sight of both monochromators is perpendicular to the accelerator axis z. Among the probable impurities, the singly and doubly ionized carbon spectral lines seem to be the most intense lines behind the current-sheet when lucite is used as an insulator. Figure 7 shows typical photoelectric signals of the C II 4267 Å line at z = 7 cm and z = 15 cm (insulator wall is at z = 0), respectively. As can be seen, the first arriving peak which is sharp and has a relatively low amplitude is followed by a high and broad second pulse. The initial carbon line signal coincides with the current-sheet and the second peak with the flow of ablated carbon atoms from the insulator. The propagation velocity of each pulse can be derived from the time delay as measured on the oscillogram. The flow velocity of the ablated material is found to be very close to that of the current-sheet. A similar recording with a 6 kV charging voltage shows the second peak to be very low in amplitude compared with the first peak in contrast to the 10 kV case described above. The third peak on the

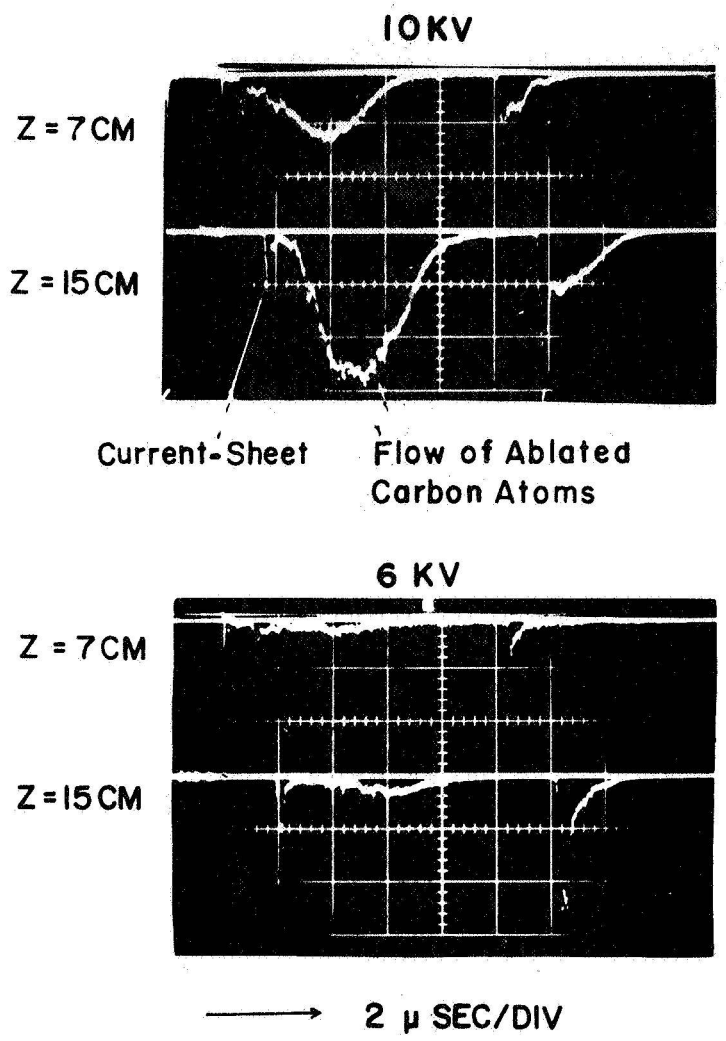

FIG. 7 PHOTOELECTRIC SIGNALS OF CII 4267 Å AT z = 7 cm AND z = 15 cm SHOWING ABLATED MATERIAL FLOW BEHIND THE CURRENT-SHEET.

oscillogram is the current-sheet produced by a reversed discharge of the second half cycle.

In order to check the carbon ion formation near the insulator wall, a monochromator is focused so as to look primarily at a portion of the volume in the vicinity of the insulator wall. This is done by observing the plasma from the back of the accelerator through the insulating disc. The photoelectric signals of the C III 4647 Å line are shown in Fig. 8 where the discharge current waveforms are also recorded. The peaks of both the C II and C III lines signals coincide with the discharge current maximum in time, and the amplitude of the signal is negligibly small at the beginning and the end part of the first half cycle. A comparison with 6 kV data indicates that far less ablation takes place at the lower discharge current.

The same spectroscopic observations are made with vycor glass used as an insulator. The carbon line signals appear to be negligibly small and do not form a distinct second peak when the system is clean. Possible silicon lines are also examined but these line signals are found to be very small. The same observations were made in an accelerator with an alumina insulator. The carbon impurity signal following the current-sheet was found as in the case with lucite. When the insulator disc was removed, it was found that the surface was covered with a black material apparently carbon impurity. This is probably due to the fact that the surface of the material is not as smooth as that of glass and the deposit of impurity is built up shot after shot. The above observations although qualitative, confirm that the carbon impurities are produced as a result of insulator wall ablation and that the current-sheet is followed by a flow of ablated material, apparently consisting of singly and doubly ionized carbon atoms. The impurity flow from the wall is a maximum at the discharge current maximum and ceases to flow at the lower

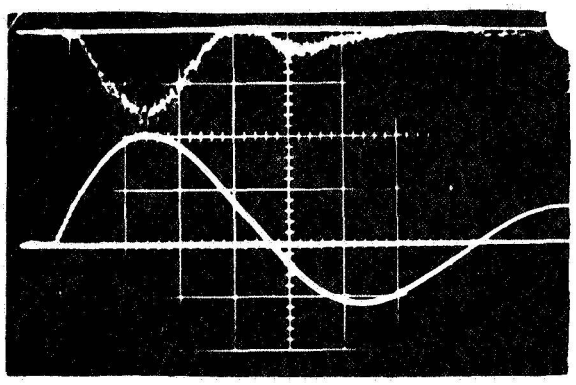

FIG. 8 SIMULTANEOUS RECORDING OF DISCHARGE CURRENT AND PHOTOELECTRIC SIGNALS CIII 4247 Å OBSERVED IN THE VICINITY OF THE INSULATOR WALL.

current, e.g., at the beginning and the end of the first cycle.

A magnetic probe is used to measure the azimuthal field B_θ in order to determine the proportion of current carried in the current-sheet. The integrated probe signals with lucite and vycor glass insulators are compared in Fig. 9, it is seen that the signal waveforms are different, i.e., the current carried in the current-sheet in the case of the lucite insulator is very small compared to the case of the vycor glass insulator and a considerable portion of the discharge current is conducted in the region behind the current-sheet, probably through the ablated material. Figure 10 shows the measured radial current in the annulus with two different capacitor charging voltages. In the 10 kV case, the current carried by the sheet is less than 50 percent, whereas about 80 percent of the total discharge current is carried in the case of 6 kV. This is as expected from the fact that far less ablation takes place with the low discharge current.

According to Keck's[13] model, a thin standing arc zone adjacent to the insulator wall exists. This is examined with frame photographs from an image converter camera taken of this region. For this, a parallel plate accelerator is used, allowing direct observation. The electrodes are separated by a lucite insulator and the gap is 3 cm. The quarter cycle time of the discharge is 2 μsec in this case. In Fig. 11, one can clearly see immediately adjacent to the insulator a discharge column which gets brighter near the current maximum in time and becomes dim thereafter. This supports the existence of a standing arc zone as predicted by Keck and the fact that the ablation takes place as a result of energy transfer from the standing arc to the insulator wall, and the vaporized gas (possibly mostly ionized) is accelerated by a Lorentz force in the arc. If the energy transfer is simply in the form of heat, the maximum temperature of the insulator wall may be in the order of 800°C.

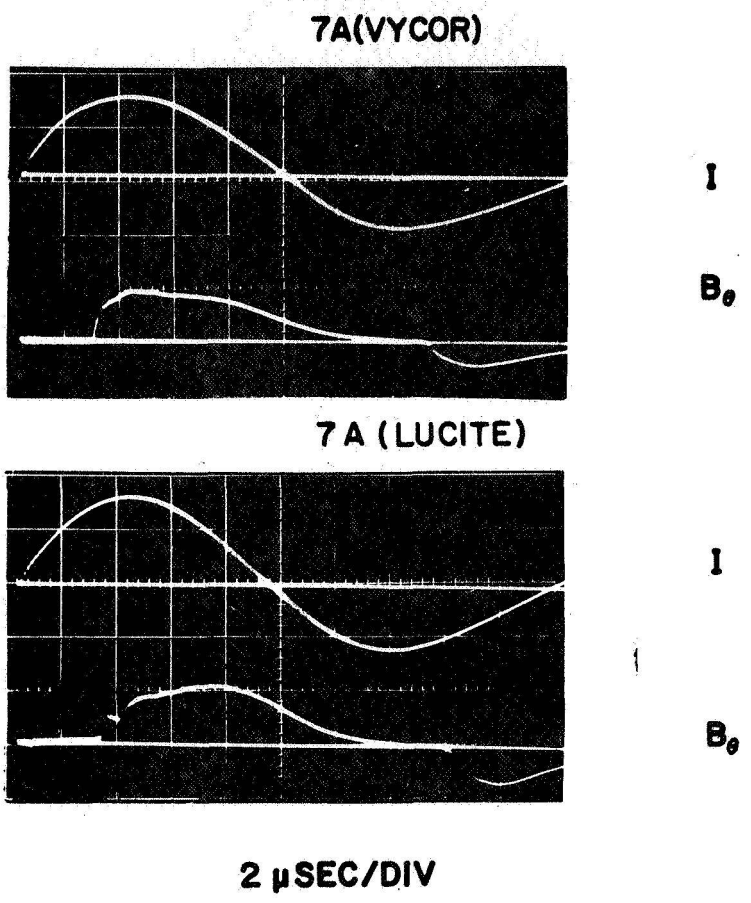

FIG. 9 COMPARISON OF MAGNETIC PROBE SIGNAL IN ACCELERATOR 7A WITH VYCOR GLASS AND LUCITE INSULATOR.

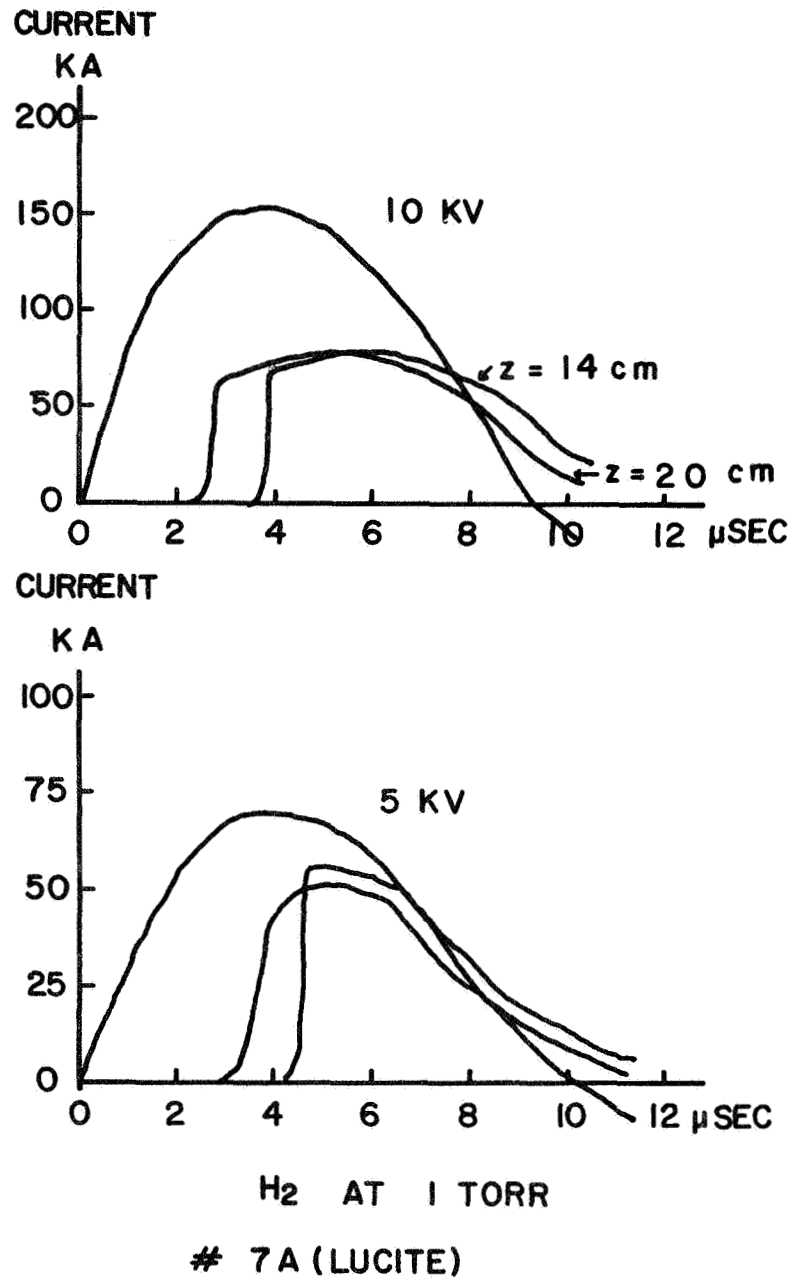

FIG. 10 SKETCH OF DISCHARGE CURRENT AND INTEGRATED PROBE SIGNALS COMPARING BETWEEN TWO DIFFERENT CHARGING VOLTAGES IN ACCELERATOR 7A (WITH LUCITE INSULATOR).

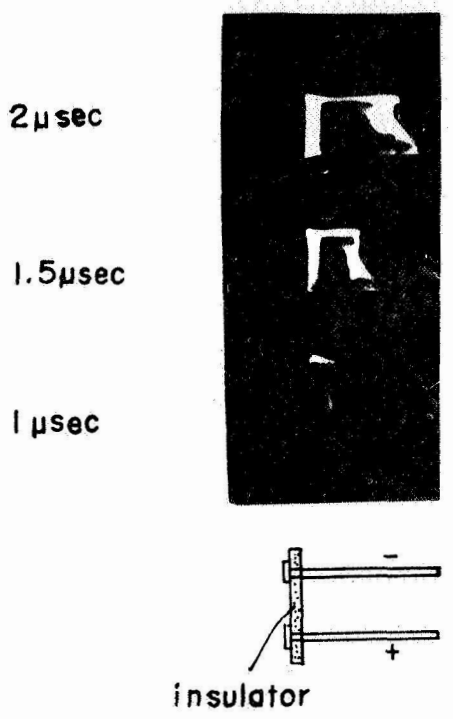

FIG. 11 FRAMING PHOTOGRAPH TAKEN WITH A PARALLEL PLATE ACCELERATOR SHOWING STANDING ARC IN THE VICINITY OF INSULATOR WALL.

D. Comparison with Workman's Theory

Workman[14] has developed a theory for the insulator ablation, which is based on the physical model proposed by Keck. The conclusion of the analysis is that the ratio of observed velocity U_p to the ideal velocity U_o is determined by the parameter $\beta = 2\epsilon_x/(m_A \cdot U_o^2)$, where ϵ_x and m_A are respectively the ionization potential and the atomic weight of the insulator material. The vaporization energy of the insulator material is assumed to be negligible compared to the ionization energy. The ideal velocity U_o is the velocity that corresponds to the case of no ablation and is related to the magnetic field B_o and the initial density ρ_g by the Kemp and Petschek's[17] expression of $B_o^2/2\mu_o = (4/3)\rho_g U_o^2$, where $B_o = \mu_o I_o/2\pi r$.

Workman's result is examined experimentally under a wide variety of conditions of accelerator operations. Figure 12 illustrates the comparison between the theory and the experimental data. The value of β is changed mainly by varying the initial gas density. One notices that all of the points deviate considerably from the theoretical curve but a set of U_p/U_o values for each accelerator falls on a curve which is roughly parallel to the theoretical curve. This implies that Workman's analysis does not take into consideration the geometric effect, i.e., the radius ratio of the accelerator electrode. As can be seen in Fig. 12, the values of U_p/U_o with 7C($r_2/r_1 = 1.5$) are generally much larger than that with 7A ($r_2/r_1 = 2.7$) for the same β. A similar result is also obtained using accelerators with a vycor glass insulator and therefore this is not related to insulator ablation.

According to the ideal velocity relation, $U_o \propto B_o\,(r_1)$ and U_o decreases as the

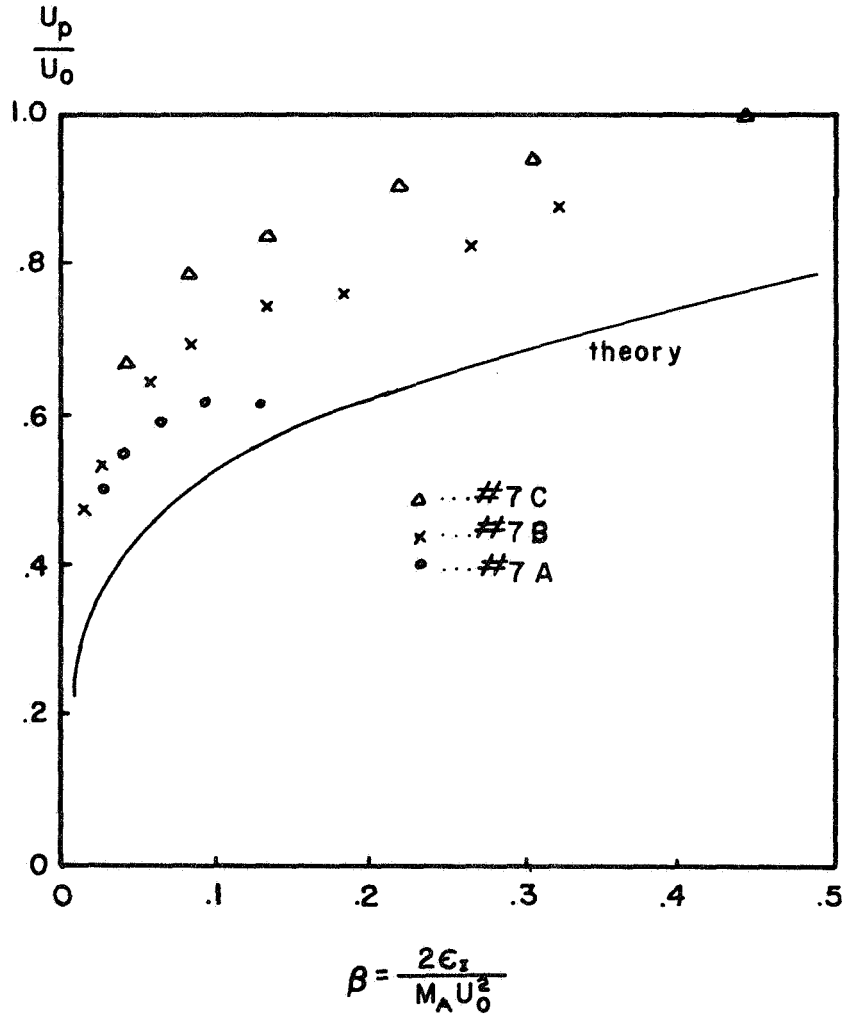

FIG. 12 PLOT OF VELOCITY RATIO U_p/U_0 AGAINST A PARAMETER ß SHOWING COMPARISON BETWEEN THE THEORY AND MEASURED VALUES.

radius of the inner electrode increases according to r_1^{-1}. The current-sheet velocity measurements with Accelerators 7A, 7B and 7C, in which only the diameter of the inner electrode differ, is made to further clarify this problem. The charging voltage, species of gas, and initial gas density are kept the same and the same insulator material is used for the measurement. The result is shown in Fig. 13, where an arbitrary curve of r^{-1} is also shown for comparison. The measured values are off from the r_1^{-1} curve within the r_2, r_1 combination used here, i.e., the velocity decreases only slightly while the radius r_1 increased from 11 mm to 20 mm. It is apparent then that the disagreement between Workman's theory and the present experiment is due to the expression of the ideal velocity (Kemp and Petschek's) used in his analysis, which is not sufficient to reflect the geometric effect of a coaxial accelerator. There has been an analysis where the effect of radius ratio of a coaxial accelerator was included[18].

E. Current-Sheet Velocity

A model of the current-sheet motion in a coaxial accelerator in which the geometry of the accelerator is better indicated may be obtained from a simplified analysis of the snowplow model. Considering the ratio of mass accumulation in the current-sheet, the equation of motion is expressed by

$$\frac{d}{dt}\left(m\frac{dz}{dt}\right) = (1/2)I^2 \frac{\partial L}{\partial z} \tag{10}$$

and $L = L_o + L'z$

$m = S \cdot \rho_o \cdot z$

where L_o represents the parasitic inductance of the external circuit, $L' = 2\ln(r_2/r_1)$ the inductance per unit length of the electrode, $S = \pi(r_2^2 - r_1^2)$ the cross section of the

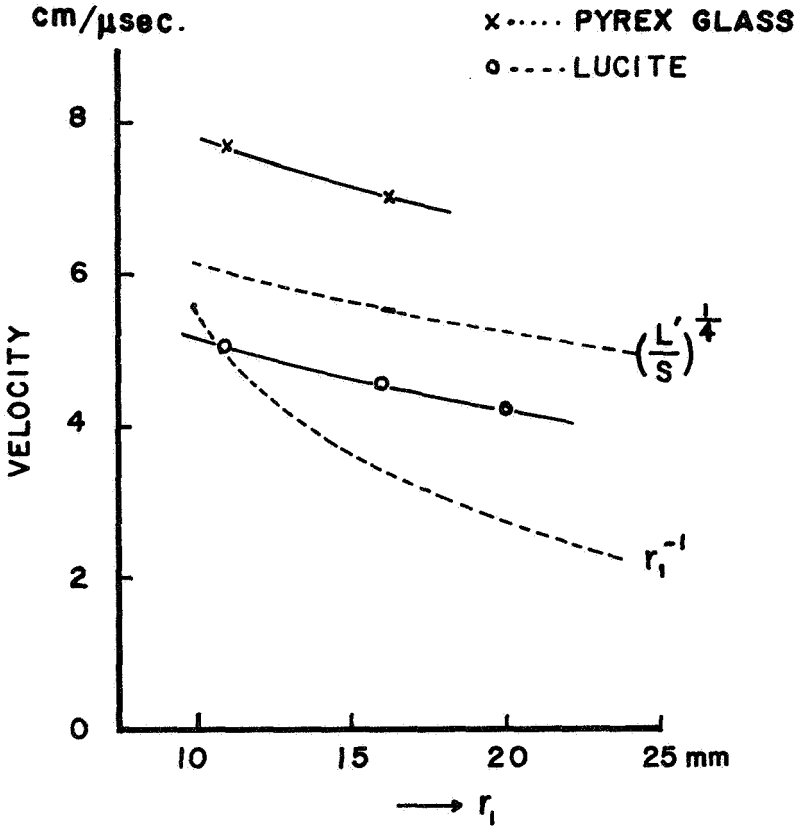

FIG. 13 CURRENT-SHEET VELOCITY AS A FUNCTION OF INNER ELECTRODE RADIUS r_1.

accelerator annulus, and I, the discharge current. Equ. (10) becomes

$$\frac{S \rho_o}{2} \frac{d^2 z^2}{dt^2} = \left(\frac{L'}{2}\right) I^2 \tag{11}$$

using $I = -CdV/dt$, $V = d/dt(L_o + L' \cdot z)I$, and also taking two simplifying assumptions, i.e., the capacitor voltage V_o to be constant during the acceleration and $L_o \gg L'.z$. The velocity of the current-sheet is then given by[19]

$$\frac{dz}{dt} = \left[\frac{4L'(V_o.z)^2}{3S \rho_o L_o^2} \right]^{1/4} \tag{12}$$

Although the above expression is not strictly quantitative due to the assumptions made, it gives a useful relation for accelerator parameters such as L', S, ρ_o, z and V_o. L' and S are determined from a combination of r_2 and r_1 in a coaxial accelerator. In Fig. 13 a curve of $(L'/S)^{1/4}$ is plotted and one sees the parametric agreement with the experimental velocities. Furthermore, the current-sheet velocities are plotted against initial gas density for hydrogen, nitrogen and argon. As can be seen in Fig. 14, there exists a slight discrepancy[14] between the curves for hydrogen and argon; however, the measured points fall approximately on a $\rho^{-1/4}$ curve within the density range used here. The velocities are measured also by changing the charging voltage of the capacitor from 6 kV to 10 kV. The results show roughly $U \propto (V_o)^{1/2}$, in agreement with previous work[20].

F. Conclusion

A direct cause for the velocity drag in the coaxial plasma accelerator where non-refractory material is used as an insulator is that the radial current in the current-sheet is very small being only a fraction of the total discharge current.

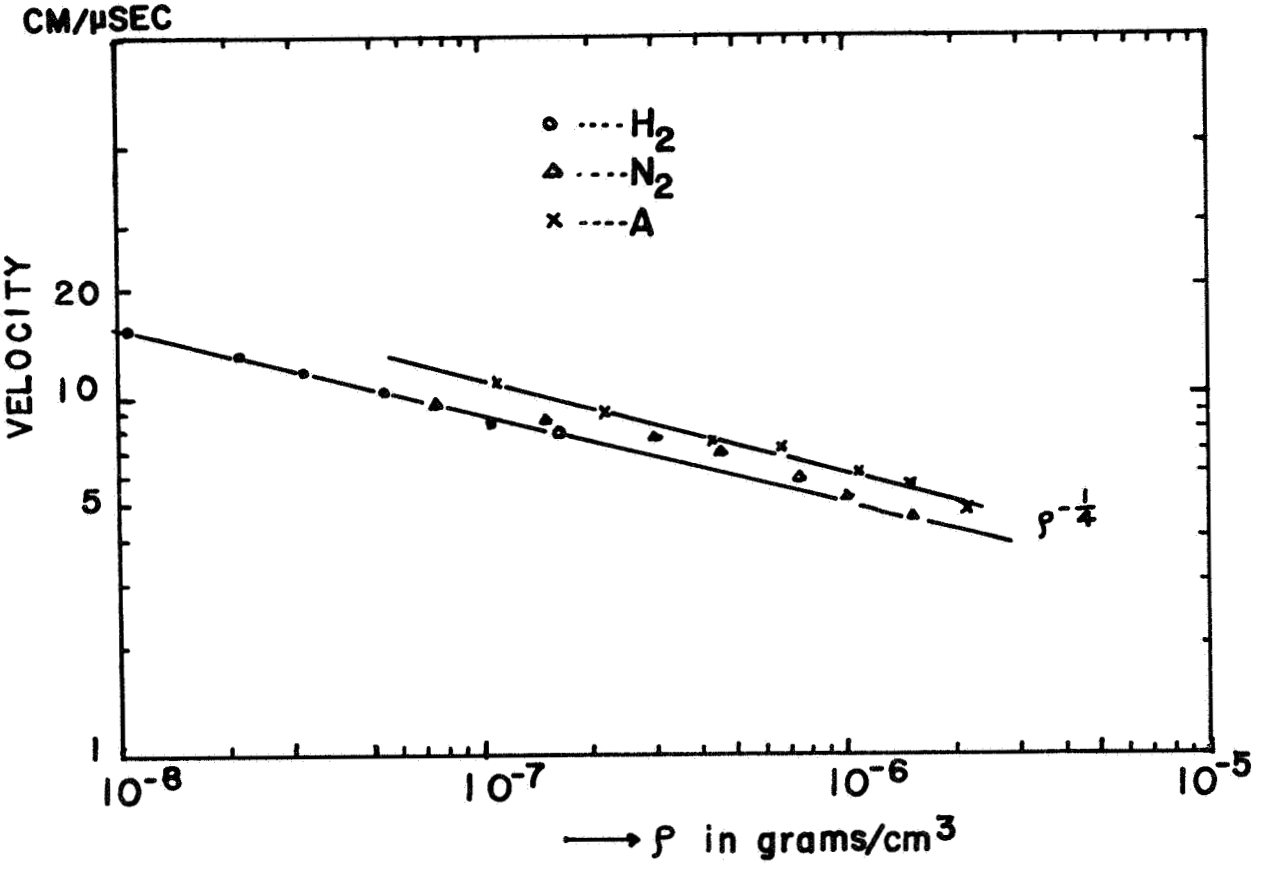

FIG. 14 CURRENT-SHEET VELOCITY AS A FUNCTION OF INITIAL GAS DENSITY.

The mass flow of insulator wall material (mainly ionized carbon) which follows the accelerating current-sheet is observed. A thin standing arc adjacent to the insulator wall is also confirmed from the frame photographs taken in a parallel plate accelerator. The ablation process is therefore a result of energy transfer (e.g. heat) from the standing arc to the wall, and vaporized wall material is ionized and accelerated through the arc up to the sheet velocity. The flow rate of ablated gas from the wall sensitively depends on the total discharge current, or possibly the current through the standing arc. The experimental observations described above support Keck's proposed model of the ablation process. Workman's analysis on the ablation is examined using the three accelerators.

The theory does not agree well with the experimental values and the cause for the failure is considered to be Kemp and Petschek's velocity relation used in the analysis which does not reflect the geometric effect of the accelerator. The velocity relation shown in equation (12) seems to agree with such parameter change as radii combinations of inner and outer electrodes, the initial gas density, and the charging voltage of the capacitor. However, it is obvious that such a simple snowplow relation does not account for the complex flow actually present particularly due to the large current path through ablating insulator. Therefore, a further study is needed to develop quantitative theory which combines appropriate snowplow model with the ablation theory.

REFERENCES

1. H.R. Griem, Plasma Spectroscopy (McGraw-Hill Book Co, Inc., New York 1964).

2. R. Wilson, J. Quant. Spectrosc. Radiat. Transfer 2, 477 (1962).

3. R.W.P. McWhirter, a paper included in A Survey of Phenomena in Ionized Gases, (International Atomic Agency, Vienna 667 (1969)).

4. D.R. Bates, A.E. Kingston, and R.W.P. McWhirter, Proc. Roy. Soc. (London) A 267, 297 (1962).

5. R. Mewe, Brit. J. Appl. Phys. 18, 107 (1967).

6. R.C. Isler and D.E. Kerr, Phys. Fluids 8, 1176 (1965).

7. M. Cloupeau, Phys. Fluids 6, 679 (1963).

8. H.R. Griem and K.Y. Shen, Phys. Rev. 122 1490 (1961); H.R. Griem, M. Branger, A.C. Kolb and G. Oertel, Phys. Rev. 125 177 (1962).

9. E.A. McLean, C.E. Faneuff, A.C. Kolb and H.R. Griem, Phys. Fluids 3 843 (1960).

10. J.R. Greig, and G. Palumbo, Phys. Fluids 12, 1211 (1969).

11. H.W. Drawin, and P. Felenbok, Data for Plasma in Local Thermodynamic Equilibrium (Gauthier-Villars Editeur, Paris 1965).

12. K. Thom, J. Norwood, and N. Jalufka, Phys. Fluids 7, S67 (1964).

13. J. Keck, Phys. Fluids 7, S16 (1964).

14. J.B. Workman, Phys. Fluids 8, 2162 (1965).

15. J.W. Mather and A.H. Williams, Rev. of Sci. Instr. 31, 297 (1960).

16. T.N. Lie, A.W. Ali, E.A. McLean and A.C. Kolb, Phys. Fluids 10, 1545 (1967).

17. N.H. Kemp and H.E. Petschek, Phys. Fluids 2, 599 (1959).

18. F.J. Fishman and H. Petschek, Phys. Fluid 5, 632 (1963).

19. L.A. Artsimovich, "Controlled Thermonuclear Reaction", (Gordon and Breach Science Publishers, New York 1964).

20. J.W. Mather, Phys. Fluids 8, 366 (1965).